Cooling of macroscopic mechanical resonators in hybrid atom-optomechanical systems

Xi Chen,[1] Yong-Chun Liu,[1] Pai Peng,[1] Yanyan Zhi,[1,2] and Yun-Feng Xiao[1,2,*]

[1]*State Key Laboratory for Mesoscopic Physics and School of Physics, Peking University, Beijing 100871, People's Republic of China*

[2]*Collaborative Innovation Center of Quantum Matter, Beijing 100871, People's Republic of China*

(Received 25 July 2015; published 22 September 2015)

Cooling macroscopic objects is of importance for both fundamental and applied physics. Here we study the optomechanical cooling in a hybrid system which consists of a cloud of atoms coupled to a cavity optomechanical system. On one hand, the asymmetric Fano or electromagnetically induced transparency resonance is explored and the steady-state cooling limits of resonators with frequency $\omega_{\rm m}$ are analytically obtained, permitting ground-state cooling of massive low-frequency resonators beyond the resolved sideband limit. On the other hand, due to the excitation-saturation effect, the validity of cooling requires the number of atoms to be much larger than the number of steady-state excitations, which is proportional to $\omega_{\rm m}^{-2}$. Thus, this limitation plays a minor role in cooling higher-frequency resonators, but becomes important for macroscopic lower-frequency resonators. Under such limitation on the number of atoms, the optimal parameters are quantified. Our study can be a guideline for both theoretical and experimental study of cooling macroscopic objects in atom-optomechanical hybrid systems.

DOI: 10.1103/PhysRevA.92.033841 PACS number(s): 42.50.Wk, 07.10.Cm, 42.50.Lc

I. INTRODUCTION

In cavity optomechanics [1–6], mechanical resonators can be cooled to the level of the quantum ground state [7–10], which promises important applications in information processing [11–17], precision control and measurement [18–23], and testing of the quantum-classical boundary [24–27]. In some real-world devices, such as the Laser Interferometer Gravitational-Wave Observatory (LIGO), the resonators to be cooled are macroscopic and of low mechanical frequency. However, the general dispersive ground-state cooling schemes require the resolved sideband limit [28–32], i.e., the cavity decay rate smaller than the mechanical frequency, which prevents ground-state cooling of massive mechanical resonators.

In recent years, a few efforts have been made on optomechanical cooling beyond the resolved sideband limit, such as cooling with dissipative coupling [33–37], optomechanically induced transparency [38,39], coupled-cavity configurations [40–42], and atom-optomechanical systems [43–52]. Among these schemes, atom-optomechanical systems are of particular interest due to the narrow linewidth of atoms for cooling in the highly unresolved sideband regime, and the experiment feasibility of coupling atoms to cavity photons [46,52–54]. However, the limitations, for example, the minimum mechanical frequency for ground-state cooling, remain unknown. In this work, we analytically study the cooling properties of the hybrid atom-optomechanical systems [Fig. 1(a)]. By analyzing the optical force spectrum, the Fano-like and the electromagnetically induced transparency (EIT)-like optical force spectrum can be observed depending on different system parameters, and the case with the EIT-like spectrum leads to more effective cooling for a weak atom-cavity coupling strength. In this case, we obtain explicit steady-state cooling limits of mechanical resonators with frequency $\omega_{\rm m}$ by solving the covariance equations of the master equation. In particular, to make the cooling model valid, the excitation-saturation effect leads to a "collective excitation number" (N_0), which is closely related to the number of atoms required. Since $N_0 \propto \omega_{\rm m}^{-2}$, N_0 can be rather small in cooling of high-frequency resonators, but becomes larger for cooling macroscopic lower-frequency resonators. Finally, we derive the full expressions of the optimal parameters.

II. SYSTEM MODEL

A hybrid atom-optomechanical system is presented in Fig. 1(a). An optical cavity mode a (with frequency $\omega_{\rm a}$ and decay rate κ) is coupled to a mechanical mode b (with frequency $\omega_{\rm m}$ and damping rate $\gamma_{\rm m}$) by optical force, and N identical ground-state two-level atoms (with transition frequency $\omega_{\rm c}$ and linewidth $\gamma_{\rm c}$) are trapped in the cavity, interacting with the light field. The cavity is driven by an input laser with frequency $\omega_{\rm L}$. The full Hamiltonian of the system and the reservoir reads [41,43]

$$H = H_0 + H_{\rm I} + H_{\rm pump} + H_{\rm bath}, \tag{1}$$

where

$$H_0 = \omega_{\rm a} a^\dagger a + \omega_{\rm m} b^\dagger b + \omega_{\rm c} S_z, \tag{2a}$$

$$H_{\rm I} = \bar{g}_0 (S_- a^\dagger + S_+ a) + g a^\dagger a (b^\dagger + b). \tag{2b}$$

The first part H_0 is the free Hamiltonian of the cavity mode, the mechanical oscillator, and the atoms. The $a^\dagger(a)$ and $b^\dagger(b)$ denote the creation (annihilation) bosonic operators of the optical and mechanical mode, and $S_z = \sum_{i=1}^{N} \sigma_z^{(i)}$ is the collective z- spin operator of the atoms. The second term $H_{\rm I}$ describes the optomechanical and the atom-field interaction, where $\bar{g}_0 = \sum_{i=1}^{N} g_0^{(i)}/N$ represents the averaged atom-photon coupling strength with $g_0^{(i)}$ being the single-photon coupling strength of the ith atom, and g is the single-photon optomechanical coupling strength. The coherent pumping of the optical mode is described by $H_{\rm pump} = \Omega^* a + \Omega a^\dagger$, where Ω is the pumping strength. The last term, $H_{\rm bath}$, describes the system-reservoir interaction, which results in the dissipations of the system. The expression of $H_{\rm bath}$ will not be shown

*Corresponding author: yfxiao@pku.edu.cn; www.phy.pku.edu.cn/~yfxiao/index.html

explicitly here, but its effect will be included in the quantum Langevin equations.

The spin algebra of the atoms can be transformed to a collective bosonic operator, $c = S_-/\sqrt{N}$. For a sufficiently large atom number N and a weak atom-photon coupling $\bar{g}_0$, $S_z \approx -N/2 + c^\dagger c$. We can apply a displacement transformation to linearize the Hamiltonian, $a \to \alpha + a$, $b \to \beta + b$, $c \to \xi + c$, where α, β, ξ are c numbers denoting the steady-state displacements of the optical, mechanical, and collective atomic modes. The linearized Hamiltonian in the frame rotating at input laser frequency ω_L is

$$H_L = -\Delta_a a^\dagger a - \Delta_c c^\dagger c + \omega_m b^\dagger b + G(a^\dagger + a)(b^\dagger + b) + G_0(a^\dagger c + c^\dagger a), \quad (3)$$

where $G_0 = \bar{g}_0\sqrt{N}$ is the collective atom-photon coupling strength, and $G = |\alpha g|$ is the cavity-enhanced optomechanical coupling strength, where the phase of α has been incorporated into the operators. $\Delta_a = \omega_L - \omega_a + 2G^2/\omega_m$ is the optomechanical-coupling modified detuning from the cavity resonance, and $\Delta_c = \omega_L - \omega_c$ is the laser detunings from the atomic resonance.

Using the linearized Hamiltonian, H_L, and taking into account the effect of the thermal bath, H_{bath}, the system quantum Langevin equations read

$$\dot{a} = \left(i\Delta_a - \frac{\kappa}{2}\right)a - iG(b^\dagger + b) - iG_0 c - \sqrt{\kappa}a_{in}, \quad (4a)$$

$$\dot{b} = \left(-i\omega_m - \frac{\gamma_m}{2}\right)b - iG(a + a^\dagger) - \sqrt{\gamma_m}b_{in}, \quad (4b)$$

$$\dot{c} = \left(i\Delta_c - \frac{\gamma_c}{2}\right)c - iG_0 a - \sqrt{\gamma_c}c_{in}. \quad (4c)$$

The corresponding noise operators a_{in}, b_{in}, and c_{in} satisfy correlations $\langle a_{in}(t)a_{in}^\dagger(t')\rangle = \langle c_{in}(t)c_{in}^\dagger(t')\rangle = \delta(t - t')$, $\langle a_{in}^\dagger(t)a_{in}(t')\rangle = \langle c_{in}^\dagger(t)c_{in}(t')\rangle = 0$, $\langle b_{in}(t)b_{in}^\dagger(t')\rangle = (n_{th} + 1)\delta(t - t')$, and $\langle b_{in}^\dagger(t)b_{in}(t')\rangle = n_{th}\delta(t - t')$. To analyze the steady-state cooling, it is preferred to transform Eq. (4) to the frequency domain:

$$\frac{\tilde{a}(\omega)}{\chi_a(\omega)} = -iG[\tilde{b}^\dagger(\omega) + \tilde{b}(\omega)] - iG_0\tilde{c}(\omega) - \sqrt{\kappa}\tilde{a}_{in}(\omega), \quad (5a)$$

$$\frac{\tilde{c}(\omega)}{\chi_c(\omega)} = -iG_0\tilde{a}(\omega) - \sqrt{\gamma_c}\tilde{c}_{in}(\omega), \quad (5b)$$

$$\frac{\tilde{b}(\omega)}{\chi_m(\omega)} = -iG[\tilde{a}(\omega) + \tilde{a}^\dagger(\omega)] - \sqrt{\gamma_m}\tilde{b}_{in}(\omega), \quad (5c)$$

where $\chi_a(\omega)^{-1} = -i(\omega + \Delta_a) + \kappa/2, \chi_c(\omega)^{-1} = -i(\omega + \Delta_c) + \gamma_c/2, \chi_m(\omega)^{-1} = -i(\omega - \omega_m) + \gamma_m/2$ are corresponding susceptibilities.

III. COOLING ENHANCED BY GROUND-STATE ATOMS

In Fig. 1(b), we present the energy levels of the coupled system in the displaced frame. Due to the atom-photon coupling, quantum interference may take place among different excitation processes. For example, interference exists between

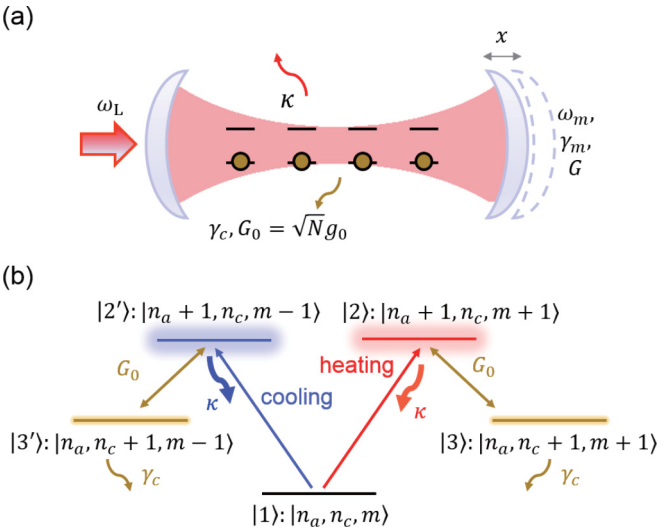

FIG. 1. (Color online) (a) An optomechanical system with a cloud of ground-state atoms coupled to an optical cavity mode. The optical mode is coherently driven by an input laser. (b) The energy-level diagram of the system in the displaced frame. $|n_a, n_c, m\rangle$ represents a state of the whole system with n_a photons, n_c atomic excitations, and m phonons. The destructive quantum interference can take place between the excitation $|1\rangle \to |2\rangle$ and $|1\rangle \to |2\rangle \to |3\rangle \to |2\rangle$ to suppress heating, similar to the constructive interference between the two cooling excitation processes, $|1\rangle \to |2'\rangle$ and $|1\rangle \to |2'\rangle \to |3'\rangle \to |2'\rangle$, to enhance cooling.

the heating excitations $|1\rangle \to |2\rangle$ and $|1\rangle \to |2\rangle \to |3\rangle \to |2\rangle$, as well as the cooling excitations $|1\rangle \to |2'\rangle$ and $|1\rangle \to |2'\rangle \to |3'\rangle \to |2'\rangle$. Thus, we could harness the interference to suppress the excitations of heating and to enhance the cooling excitations. This effect may enable efficient cooling even in the highly unresolved sideband regime, $\kappa \gg \omega_m$.

Intuitively, there are two cooling schemes for this system. The sketches shown in the insets of Figs. 2(a) and 2(b) indicate that, for the narrow atomic linewidth, $\gamma_c \ll \omega_m$, the atoms can modulate the cavity profile either at the red sideband to increase the cooling rate by the constructive quantum interference or at the blue sideband to suppress the heating rate by the destructive quantum interference. Using Eq. (5), we calculate the optical force spectrum $S_{FF}(\omega) = \int_{-\infty}^{\infty} \tilde{F}^\dagger(\omega)\tilde{F}(\omega')d\omega'$, where the optomechanical force in the frequency domain is $\tilde{F}(\omega) = -G[\tilde{a}(\omega) + \tilde{a}^\dagger(\omega)]/x_{ZPF}$, with x_{ZPF} denoting the zero-point fluctuation of the resonator. The cooling and heating rates $A_\mp$ can be expressed as $A_- = S_{FF}(\omega_m)x_{ZPF}^2$ and $A_+ = S_{FF}(-\omega_m)x_{ZPF}^2$. The full expression of $S_{FF}(\omega)$ reads

$$S_{FF}(\omega) = \frac{G^2}{x_{ZPF}^2}|\chi(\omega)|^2\left(\kappa + \gamma_c G_0^2|\chi_c(\omega)|^2\right), \quad (6)$$

where $\chi(\omega)^{-1} = \chi_a(\omega)^{-1} + G_0^2\chi_c(\omega)$ accounts for the total susceptibility of the optical and atomic mode. For the highly unresolved sideband regime, $\kappa \gg \omega_m$, the system can be approximated by the atomic mode c, the mechanical mode b, and an effective coupling between them (see Appendix A), having the following effective system

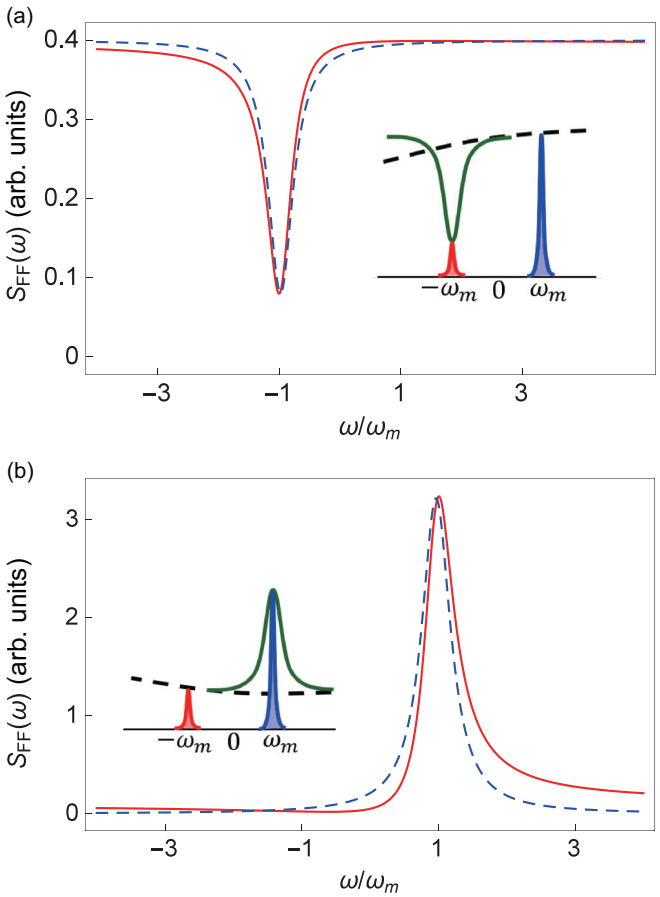

FIG. 2. (Color online) EIT and Fano line shapes of the optical force spectrum $S_{\rm FF}(\omega)$ under $|\Delta_{\rm a}| \ll \kappa$ and $|\Delta_{\rm a}| > \kappa$, respectively. In [(a) or (b)], the blue dashed and red solid curves represent $S_{\rm FF}^{\rm EIT}(\omega)$ [or $S_{\rm FF}^{\rm Fano}(\omega)$] and $S_{\rm FF}(\omega)$. Insets: Sketches of the cavity profile modulated by the atoms. The black dashed curves denote the cavity line shape and the green solid curves represent the line shape of the atoms. The heights of red and blue peaks at $-\omega_{\rm m}$ and $\omega_{\rm m}$ correspond to the heating and cooling rates. The parameters are $\kappa = 10^5\omega_{\rm m}$, $\gamma_{\rm c} = 0.1\omega_{\rm m}$, $G_0 = 100\omega_{\rm m}$, $G = 100\omega_{\rm m}$, $\Delta_{\rm a} = 5000\omega_{\rm m}$, and $\Delta_{\rm c} = \omega_{\rm m}$ in (a) and $\kappa = 10^4\omega_{\rm m}$, $G_0 = 200\omega_{\rm m}$, $G = 100\omega_{\rm m}$, $\Delta_{\rm c} = 0.3\omega_{\rm m}$, and $\Delta_{\rm a} = J^2/(\Delta_{\rm c} + \omega_{\rm m})$ in (b).

parameters ($\Delta_{\rm a} \gg \Delta_{\rm c}$):

$$\kappa_{\rm eff} = \gamma_{\rm c} + \eta^2\kappa, \tag{7a}$$

$$\Delta_{\rm eff} = \Delta_{\rm c} - \eta^2\Delta_{\rm a}, \tag{7b}$$

$$G_{\rm eff} = \eta G, \tag{7c}$$

$$\eta = \frac{G_0}{\sqrt{\left(\frac{\kappa}{2}\right)^2 + \Delta_{\rm a}^2}}. \tag{7d}$$

The optical force spectrum can also be modulated by the cavity detuning $\Delta_{\rm a}$ for the following two cases.

(i) For the case of $\Delta_{\rm a} \ll \kappa$, the optical force spectrum can be approximated by an EIT line shape:

$$S_{\rm FF}^{\rm EIT}(\omega) \simeq S_{\rm FF}^{G_0=0}(\omega) - S_{\rm FF}^{\rm A-M}(\omega), \tag{8}$$

in which $S_{\rm FF}^{G_0=0}(\omega)$ is the optical force spectrum in the absence of atoms, and $S_{\rm FF}^{\rm A-M}(\omega) = \kappa_{\rm eff}G_{\rm eff}^2|\chi_{\rm eff}(\omega)|^2/x_{\rm ZPF}^2$ corresponds to the spectrum of the effective coupling between the atomic and mechanical modes with $\chi_{\rm eff}(\omega)^{-1} = -i(\omega + \Delta_{\rm eff}) + (\kappa_{\rm eff}/2)$. Since $S_{\rm FF}^{G_0=0}(\omega)$ is flat over a wide frequency range and $\eta^2\Delta_a \ll \omega_{\rm m}$, the optimal cooling takes place for $\Delta_{\rm eff,opt}^{\rm EIT} = \omega_{\rm m} \simeq \Delta_{\rm c}$, where the heating effect is mostly reduced due to the destructive quantum interference. The $S_{\rm FF}^{\rm EIT}(\omega)$ and the exact $S_{\rm FF}(\omega)$ for this case are displayed in Fig. 2(a), showing a good agreement.

(ii) For $\Delta_a > \kappa$, the optical force spectrum behaves as a Fano line shape:

$$S_{\rm FF}^{\rm Fano}(\omega) \simeq S_{\rm FF}^{\rm A-M}(\omega). \tag{9}$$

For this case, the optimal cooling takes place for $\Delta_{\rm eff,opt}^{\rm Fano} = -\omega_{\rm m}$. Figure 2(b) shows that $S_{\rm FF}^{\rm Fano}(\omega)$ is consistent with $S_{\rm FF}(\omega)$. The detailed deductions of Eqs. (8) and (9) can be found in Appendix B.

Considering the weak atom-photon coupling strength G_0, a small $\Delta_{\rm a}$ is preferred for sufficiently large effective optomechanical coupling $G_{\rm eff}$, corresponding to EIT line shapes (see Appendix B). Thus we will focus on the cooling properties of the EIT scheme. For the exact solution of the steady-state phonon number, we refer to the master equation [31,41]:

$$\begin{aligned}\dot\rho = {} & i[\rho, H_{\rm L}] + \frac{\kappa}{2}(2a\rho a^\dagger - a^\dagger a\rho - \rho a^\dagger a) \\ & + \frac{\gamma_{\rm c}}{2}(2c\rho c^\dagger - c^\dagger c\rho - \rho c^\dagger c) \\ & + \frac{\gamma_{\rm m}}{2}(n_{\rm th}+1)(2b\rho b^\dagger - b^\dagger b\rho - \rho b^\dagger b) \\ & + \frac{\gamma_{\rm m}}{2}n_{\rm th}(2b^\dagger\rho b - bb^\dagger\rho - \rho bb^\dagger).\end{aligned} \tag{10}$$

The time evolution of the mean phonon number $\langle b^\dagger b\rangle(t)$ can be obtained by solving the equations of second-order moments $\partial_t\langle\hat o_i\hat o_j\rangle = {\rm Tr}(\dot\rho\hat o_i\hat o_j) = \sum_{k,l}\eta_{ijkl}\hat o_k\hat o_l$, where $\hat o_{i,j,k,l}$ is one of the operators a, $a^\dagger$, c, $c^\dagger$, b, and $b^\dagger$, and coefficients η_{ijkl} can be calculated from Eq. (10). For the EIT line shapes ($\Delta_{\rm a} \ll \kappa$, $G_0^2 \ll \kappa\omega_{\rm m}$) with optimal cooling conditions $\Delta_{\rm c} = \omega_{\rm m}$, we obtain the approximate solutions of the steady-state phonon number in terms of the classical part $n_{\rm f}^{\rm c}$ and the quantum part $n_{\rm f}^{\rm q}$:

$$n_{\rm f} = n_{\rm f}^{\rm c} + n_{\rm f}^{\rm q}, \tag{11a}$$

$$n_{\rm f}^{\rm c} \simeq \frac{4G_{\rm eff}^2 + \kappa_{\rm eff}^2}{4G_{\rm eff}^2\kappa_{\rm eff}}\gamma_{\rm m}n_{\rm th}, \tag{11b}$$

$$n_{\rm f}^{\rm q} \simeq \frac{4G_{\rm eff}^2 + \gamma_{\rm c}(\kappa_{\rm eff} - \gamma_{\rm c})}{(\kappa_{\rm eff} - \gamma_{\rm c})^2}\frac{\omega_m^2}{\omega_m^2 - 4G_{\rm eff}^2 + \kappa_{\rm eff}^2/4}, \tag{11c}$$

where $4G_{\rm eff}^2\kappa_{\rm eff}/(4G_{\rm eff}^2 + \kappa_{\rm eff}^2)$ is the optomechanical damping rate, and the intrinsic damping rate $\gamma_{\rm m}$ is neglected. While the expression of classical cooling limit $n_{\rm f}^{\rm c}$ remains the same form as the case of a single cavity, the quantum part can be considerably different [31,32]. One can check that ground-state cooling still holds for $\kappa_{\rm eff} \ll \omega_{\rm m}$. The stability criterion $\omega_m^2 - 4G_{\rm eff}^2 + \kappa_{\rm eff}^2/4 > 0$ indicated by Eq. (11) is also identical to the single-cavity case. Since $G_{\rm eff} = (2G_0/\kappa)G$ and $\kappa_{\rm eff} = (4G_0^2/\kappa) + \gamma_{\rm c}$, $G_{\rm eff}$ and $\kappa_{\rm eff}$ can be tuned individually by varying G and G_0.

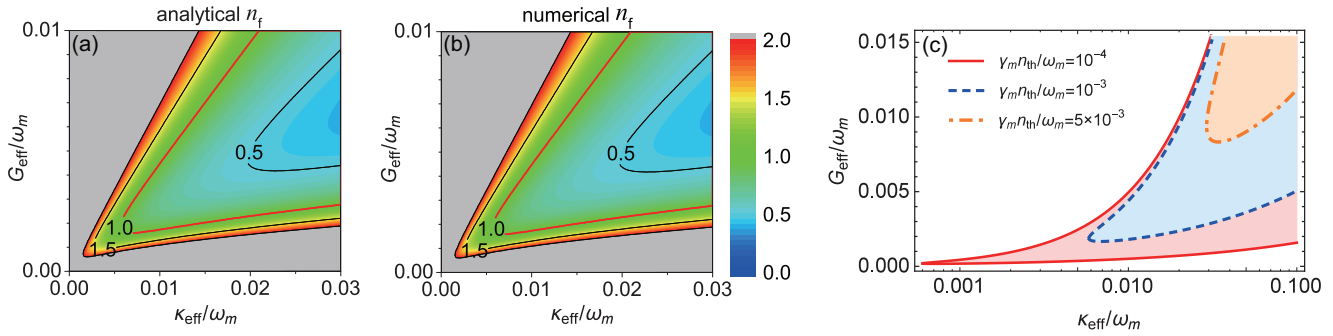

FIG. 3. (Color online) (a) Analytical and (b) numerical cooling limits n_f for $\gamma_c = 10^{-5}\omega_m \ll \gamma_m n_{th}$. (c) Ground-state cooling boundaries of κ_{eff} and G_{eff} for different $\gamma_m n_{th}$. The red solid, blue dashed, and orange dot-dashed curves, along with shaded regions, correspond to $n_f \leqslant 1$ for $\gamma_m n_{th}/\omega_m = 10^{-4}, 10^{-3}$, and 5×10^{-3}. The scale of the κ_{eff} axis is logarithmic. Other unspecified parameters are $\kappa = 10^5\omega_m$, $\gamma_m = 10^{-7}\omega_m$, $n_{th} = 10^4$, $\Delta_c = \omega_m$, and $\Delta_a = 0$.

IV. LIMITATION FOR GROUND-STATE COOLING OF MACROSCOPIC RESONATORS

The effective parameters in Eq. (7) indicate that $\kappa_{eff} \ll \omega_m$ can be achieved even in the highly unresolved sideband regime of the cavity, $\kappa \gg \omega_m$, since the lifetimes of exited states are long enough by employing cold atoms. However, for the validity of treating $c^\dagger$ as a collective bosonic excitation of atoms in Eq. (3), the steady-state atomic excitation should be much smaller than the atom number, $\xi^2 \ll N$. Since $\xi^2 = G_0^2\alpha^2/(\Delta_c^2 + \gamma_c^2)$, $\Delta_c = \omega_m$, and $\gamma_c \ll \omega_m$, the number of atoms satisfies

$$N \gg \left(\frac{\kappa}{g}\right)^2\left(\frac{G_{eff}}{2\omega_m}\right)^2. \tag{12}$$

This requirement will be strict for massive resonators of low frequency ω_m. In the following, we define the collective excitation number as $N_0 \equiv (\kappa/g)^2(G_{eff}/2\omega_m)^2$ in Eq. (12). For certain κ/g and ω_m, N_0 can be reduced by obtaining the minimal G_{eff} capable of ground-state cooling from Eq. (11).

For $G_{eff} \ll \omega_m$, $\kappa_{eff} < \omega_m$, and $(\gamma_c,\ \gamma_m n_{th}) \ll \omega_m$, Eq. (11c) can be further simplified for the following two situations regarding the atomic linewidth.

(i) $\gamma_c \ll \gamma_m n_{th}$. The quantum part of the cooling limit reduces to

$$n_f^{q,1} = 4\frac{G_{eff}^2}{\kappa_{eff}^2}. \tag{13}$$

In Fig. 3(a), we present the cooling limit $n_f = n_f^c + n_f^{q,1}$ for this case, showing a good agreement with the numerical result [Fig. 3(b)]. Figure 3(c) shows the boundaries of ground-state cooling for different $\gamma_m n_{th}$. The minimum effective optomechanical coupling strength for $n_f = 1$ can be obtained as $G_{eff} = G_{eff,1}^{min} \simeq 1.7\gamma_m n_{th}$.

(ii) $\gamma_m n_{th} \ll \gamma_c \ll \omega_m$. For this case, the quantum part of the cooling limit is

$$n_f^{q,2} = \frac{4G_{eff}^2}{(\kappa_{eff} - \gamma_c)^2} + \frac{\gamma_c}{\kappa_{eff} - \gamma_c}. \tag{14}$$

The analytical cooling limit $n_f = n_f^c + n_f^{q,2}$ for this case [Fig. 4(a)] is in accordance with the numerical result [Fig. 4(b)] as well. Figure 4(c) displays the ground-state cooling boundary for different $\gamma_m n_{th}$. The minimum effective optomechanical coupling strength can be similarly calculated as $G_{eff} = G_{eff,2}^{min} \simeq 1.2\sqrt{\gamma_c\gamma_m n_{th}}$. Comparing $G_{eff,2}^{min}$ with $G_{eff,1}^{min}$, we find that the optimal atom linewidth is $\gamma_c \ll \gamma_m n_{th}$ in order to obtain the minimum N_0.

By plugging the optimal $G_{eff,1}^{min}$ into the expression of N_0, the minimal ω_m of ground-state cooling is

$$\omega_m^{min} = 1.1 \times 10^{11}\frac{1}{\sqrt{N_0}}\frac{\kappa T}{g Q_m}. \tag{15}$$

In experiments, cold atoms with ultranarrow linewidths hold great potential for cooling low-frequency resonators, but the achievable number of atoms is limited [46,52–54], which

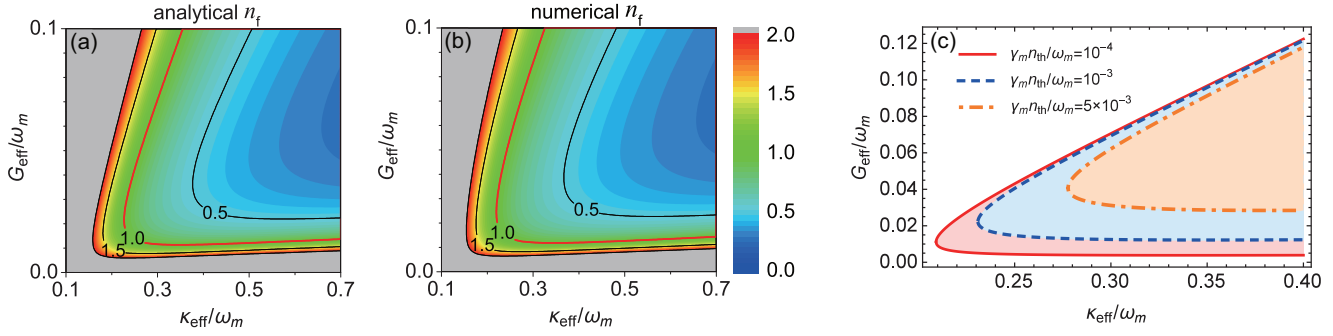

FIG. 4. (Color online) (a) Analytical and (b) numerical cooling limits n_f for $\gamma_c = 0.1\omega_m$, which satisfies $\gamma_c \gg \gamma_m n_{th}$ and $\gamma_c \ll \omega_m$. (c) Ground-state cooling boundaries of κ_{eff} and G_{eff} for different $\gamma_m n_{th}$. The red solid, blue dashed, and orange dot-dashed curves, along with shaded regions, correspond to $n_f \leqslant 1$ for $\gamma_m n_{th}/\omega_m = 10^{-4}, 10^{-3}$, and 5×10^{-3}. Other unspecified parameters are the same as those in Fig. 3.

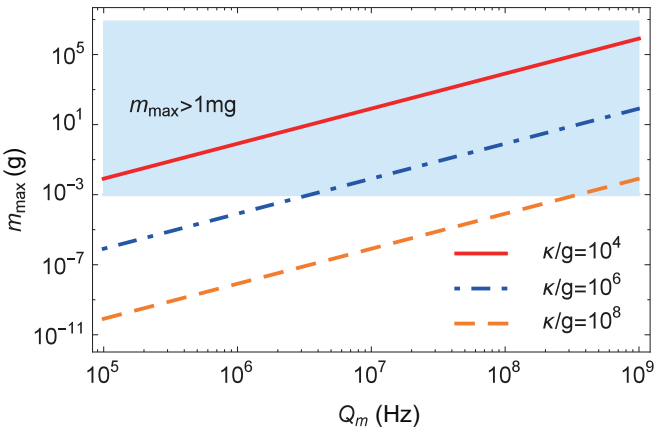

FIG. 5. (Color online) Maximum mass of the membrane for ground-state cooling at $T = 1$ mK. The red solid, blue dot-dashed, and orange dashed lines are the cases of $\kappa/g = 10^4$, 10^6, and 10^8. In the light-blue shaded region, ground-state cooling of the membranes of $m > 1$ mg can be achieved.

brings difficulties to cooling. In particular, for a reasonable $N_0 = 10^6$, $\kappa = 1$ MHz, $g = 0.01\omega_{\rm m}$, $T = 0.1$ K, and $Q_{\rm m} = 10^7$, ground-state cooling can be achieved for an object of frequency $\omega_{\rm m} = 10$ kHz.

Finally, as a concrete example, we relate $\omega_{\rm m}$ to the mass m of a Si_3N_4 membrane resonator, with mass density $\rho = 2.7$ g/cm^3. The eigenfrequency of such a membrane is given by $\omega_{\rm m}(j,k)/2\pi = \sqrt{f/4\sigma}\sqrt{j^2/l_x^2 + k^2/l_y^2}$, where $f = 50$ N/m is the tension per unit length and σ is the mass surface density [55]. Here we focus on the fundamental mode ($j = k = 1$) of a square membrane with side length l, thickness h, and $\sigma = \rho h = m/l^2$, and thus obtain

$$m_{\rm max} = 8.2 \times 10^{-20} N_0 \left(\frac{g Q_{\rm m}}{\kappa T}\right)^2. \tag{16}$$

The maximum mass of the membrane for achievable ground-state cooling is plotted in Fig. 5, with respect to the mechanical quality factor $Q_{\rm m}$ and κ/g. For example, it would be possible to cool membrane resonators with mass $m > 1$ mg, as indicated by the blue shaded region in Fig. 5, for small κ/g and large $Q_{\rm m}$ and at lower temperature.

V. CONCLUSIONS

We have studied the ground-state cooling of macroscopic mechanical resonators in a coupled atom-optomechanics system. In this system, net cooling can be enhanced by either constructive quantum interference to strengthen cooling or destructive interference to suppress heating. Using the covariances of the system master equations, the steady-state cooling limit is obtained analytically. Furthermore, to validate cooling, the number of atoms N should be much larger than the collective excitation number, i.e., $N \gg N_0$. Since $N_0 \propto \omega_{\rm m}^{-2}$, cooling of macroscopic objects might be highly challenging. The present results may provide a guideline for both theoretical and experimental study of cooling of macroscopic objects in atom-optomechanical hybrid systems.

ACKNOWLEDGMENTS

This work was supported by the 973 Program (Grants No. 2013CB328704 and No. 2013CB921904) and National Natural Science Foundation of China (Grants No. 61435001, No. 11474011, No. 11222440, and No. 11121091). X.C. was supported by the National Fund for Fostering Talents of Basic Science (Grant No. J1103205).

APPENDIX A: THE EFFECTIVE ATOM-MECHANICAL INTERACTION

The quantum Langevin equations [Eq. (4)] can be formally integrated as

$$a(t) = a(0)e^{i\Delta_{\rm a}t-\kappa t/2} + e^{i\Delta_{\rm a}t-\kappa t/2}\int_0^t \{[-iGb(\tau) - iGb^\dagger(\tau) - iG_0c(\tau) - \sqrt{\kappa}a_{\rm in}(\tau)]e^{-i\Delta_{\rm a}\tau+\kappa\tau/2}\}d\tau, \tag{A1}$$

$$b(t) = b(0)e^{-i\omega_{\rm m}t-\gamma_{\rm m}t/2} + e^{i\omega_{\rm m}t-\gamma_{\rm m}t/2}\int_0^t \{[-iGa(\tau) - iGa^\dagger(\tau) - iG_0c(\tau) - \sqrt{\gamma_{\rm m}}b_{\rm in}(\tau)]e^{i\omega_{\rm m}\tau+\gamma_{\rm m}\tau/2}\}d\tau, \tag{A2}$$

$$c(t) = c(0)e^{i\Delta_{\rm c}t-\gamma_{\rm c}t/2} + e^{i\Delta_{\rm c}t-\gamma_{\rm c}t/2} \times \int_0^t \{[-iG_0a(\tau) - \sqrt{\gamma_{\rm c}}c_{\rm in}(\tau)]e^{-i\Delta_{\rm c}\tau+\gamma_{\rm c}\tau/2}\}d\tau. \tag{A3}$$

Since the decay rate of the cavity κ is much larger than the linewidth of the atoms, by treating the optical mode a perturbatively, we obtain

$$c(t) \simeq c(0)e^{i\Delta_{\rm c}t-\gamma_{\rm c}t/2} + C_{\rm in}(t), \tag{A4}$$

$$b(t) \simeq b(0)e^{-i\omega_{\rm m}t-\gamma_{\rm m}t/2} + B_{\rm in}(t), \tag{A5}$$

where $C_{\rm in}(t)$ and $B_{\rm in}(t)$ are the integrations of noise terms. By plugging Eqs. (A4) and (A5) into Eq. (A1), we can obtain the equation of mode a. By plugging a back to Eqs. 4(b) and 4(c), with the conditions $|\Delta_{\rm a}| \gg |\Delta_{\rm c}|$, $\kappa \gg (\gamma_{\rm c}, \omega_{\rm m})$, and $\omega_{\rm m} \gg \gamma_{\rm m}$, the equation of mode c, with the effective coupling between mode b and c, can be obtained as

$$\dot{c} = \left(i\Delta_{\rm c} - \frac{\gamma_{\rm c}}{2}\right)c - iG_0\left\{-\frac{iG[b^\dagger(t)+b(t)]}{-i\Delta_{\rm a}+\kappa/2} - \frac{iG_0c(t)}{-i\Delta_{\rm a}+\kappa/2}\right\} - \sqrt{\gamma_{\rm c}}c_{\rm in} - iG_0[a(0)e^{i\Delta_{\rm a}t-\kappa t/2} + A_{\rm in}(t)], \tag{A6}$$

from which we obtain the effective parameters:

$$i\Delta_{\rm c} - \frac{\gamma_{\rm c}}{2} - \frac{G_0^2}{-i\Delta_{\rm a}+\kappa_2} \longleftrightarrow i\Delta_{\rm eff} - \frac{\kappa_{\rm eff}}{2}, \tag{A7}$$

$$\left|\frac{G_0G}{i\Delta_{\rm a}-\frac{\kappa}{2}}\right| \longleftrightarrow |G_{\rm eff}|. \tag{A8}$$

Defining $\eta = G_0/\sqrt{(\kappa/2)^2+\Delta_{\rm a}^2}$, the effective parameters can be expressed as Eq. (7).

APPENDIX B: THE EIT AND FANO LINE SHAPE

Under the conditions $|\Delta_a| \gg |\Delta_c|$, $\kappa \gg (\gamma_c,\ \omega_m)$, and $\omega_m \gg \gamma_m$ of the coupled system, the optical force spectrum [Eq. (6)] can be reduced to EIT or Fano line shape. For the weak atom-photon coupling strength, $G_0^2 \ll \kappa\omega_m$, and under $\Delta_a \ll \kappa$, the EIT line shape of the force spectrum can be obtained as

$$\begin{aligned} S_{FF}(\omega) &= \frac{G^2\left[(\omega+\Delta_c)^2+\left(\frac{\gamma_c}{2}\right)^2\right]}{\left\{\left[-i(\omega+\Delta_a)+\frac{\kappa}{2}\right]\left[-i(\omega+\Delta_c)+\frac{\gamma_c}{2}\right]+G_0^2\right\}^2}\left[\kappa+\frac{\gamma_c G_0^2}{(\omega+\Delta_c)^2+\left(\frac{\gamma_c}{2}\right)^2}\right] \\ &= \frac{G^2\left\{\kappa\left[(\omega+\Delta_c)^2+\left(\frac{\gamma_c}{2}\right)^2\right]+\gamma_c G_0^2\right\}}{\left[-(\omega+\Delta_a)(\omega+\Delta_c)+\left(\frac{\kappa}{2}\right)\left(\frac{\gamma_c}{2}\right)+G_0^2\right]^2+\left[(\omega+\Delta_a)\frac{\gamma_c}{2}+(\omega+\Delta_c)\frac{\kappa}{2}\right]^2} \\ &\simeq \frac{G^2\left\{\kappa\left[(\omega+\Delta_c)^2+\left(\frac{\gamma_c}{2}\right)^2\right]+\gamma_c G_0^2\right\}}{\left[(\omega+\Delta_a)^2+\left(\frac{\kappa}{2}\right)^2\right]\left[(\omega+\Delta_c)^2+\left(\frac{\gamma_c}{2}+\frac{2G_0^2}{\kappa}\right)^2\right]} \\ &\simeq \frac{G^2\kappa}{(\omega+\Delta_a)^2+\left(\frac{\kappa}{2}\right)^2}-\frac{G_{\rm eff}^2\kappa_{\rm eff}}{(\omega+\Delta_c)^2+\left(\frac{\kappa_{\rm eff}}{2}\right)^2} \\ &\simeq S_{FF}^{G_0=0}(\omega)-S_{FF}^{\rm eff}(\omega), \end{aligned} \tag{B1}$$

where $\Delta_{\rm eff}=\Delta_c-4G_0^2\Delta_a/\kappa\simeq\Delta_c$, and we have taken $\omega+\Delta_a\ll\kappa$. Thus, this approximated result $S_{FF}(\omega)\simeq S_{FF}^{G_0=0}(\omega)-S_{FF}^{\rm eff}(\omega)$ works well for $\omega\ll\kappa$, as presented in Fig. 2(a). For $G_0\gtrsim\kappa\omega_m$ and $\Delta_a>\kappa$, the Fano line shape of the optical force spectrum can be calculated as

$$\begin{aligned} S_{FF}(\omega) &= \frac{G^2}{\left[-i(\omega+\Delta_a)+\frac{\kappa}{2}+\frac{G_0^2}{-i(\omega+\Delta_c)+\frac{\gamma_c}{2}}\right]^2}\times\left[\kappa+\frac{\gamma_c G_0^2}{(\omega+\Delta_c)^2+\left(\frac{\gamma_c}{2}\right)^2}\right] \\ &= \frac{G^2}{\left\{-i(\omega+\Delta_c)+\frac{\gamma_c}{2}+\frac{G_0^2}{(\omega+\Delta_a)^2+\left(\frac{\kappa}{2}\right)^2}\left[i(\omega+\Delta_a)+\frac{\kappa}{2}\right]\right\}^2}\times\left\{\frac{\kappa\left[(\omega+\Delta_c)^2+\left(\frac{\gamma_c}{2}\right)^2\right]}{(\omega+\Delta_a)^2+\left(\frac{\kappa}{2}\right)^2}+\frac{\gamma_c G_0^2}{(\omega+\Delta_a)^2+\left(\frac{\kappa}{2}\right)^2}\right\} \\ &\simeq \frac{G^2}{\left[-i(\omega+\Delta_c)+\frac{\gamma_c}{2}+\eta^2\left(i\Delta_a+\frac{\kappa}{2}\right)\right]^2}(\kappa\eta^4+\gamma_c\eta^2) \\ &= \frac{\eta^2G^2(\kappa\eta^2+\gamma_c)}{\left[-i(\omega+\Delta_c-\eta^2\Delta_a)+\frac{\gamma_c+\eta^2\kappa}{2}\right]^2} \\ &= \frac{G_{\rm eff}^2\kappa_{\rm eff}}{(\omega+\Delta_{\rm eff})^2+\left(\frac{\kappa_{\rm eff}}{2}\right)^2}, \end{aligned} \tag{B2}$$

where $[(\omega+\Delta_c)^2+(\gamma_c/2)^2]/[(\omega+\Delta_a)^2+(\kappa/2)^2]$ is replaced by η^4 after applying the optimal-cooling condition for the Fano line shape, $\Delta_c-\eta^2\Delta_a\simeq-\omega_m$. This approximation also works for $\omega\ll\kappa$, as illustrated in Fig. 2(b).

For a weak atom-photon coupling strength $G_0=100\omega_m\ll\kappa\omega_m$, the numerical cooling limit n_f of Δ_a and Δ_c is presented in Fig. 6. Ground-state cooling can be achieved for $\Delta_c\simeq\omega_m$ and $\Delta_a\simeq0.2\kappa$, which is the case for the EIT line shape. For the case of the Fano line shape, cooling will be less efficient and the detunings are very close to the unstable region. Thus, the optimal cooling for weak atom-photon coupling strength is achieved in the EIT line-shape regime.

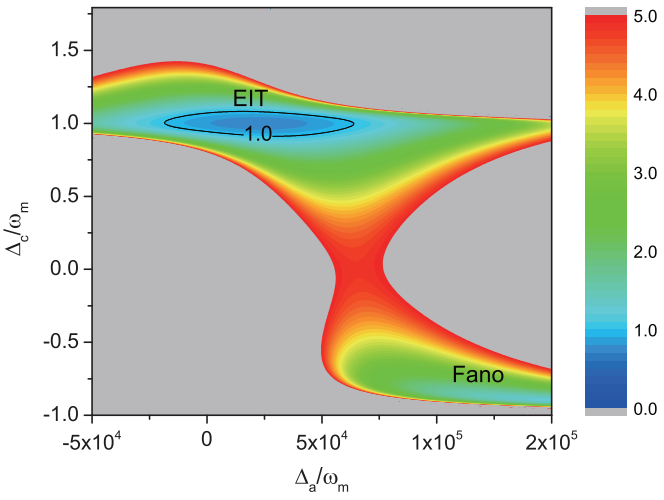

FIG. 6. (Color online) Cooling limits for different detunings. The system parameters are $\kappa=10^5\omega_m$, $\gamma_m=10^{-7}\omega_m$, $n_{th}=10^5$, $G_0=100\omega_m$, $G=0.2G_0$, and $\gamma_c=0.01\omega_m$. Gray regions correspond to the final phonon number $n_f>5$, which is close to the unstable region. For this case, ground-state cooling can only be achieved in the region around $\Delta_c=\omega_m$, $\Delta_a=0.2\kappa$, which corresponds to the parameters for an EIT line shape.

[1] T. J. Kippenberg and K. J. Vahala, Science **321**, 1172 (2008).
[2] F. Marquardt and S. M. Girvin, Physics **2**, 40 (2009).
[3] Y.-C. Liu, Y.-W. Hu, C. W. Wong, and Y.-F. Xiao, Chin. Phys. B **22**, 114213 (2013).

[4] P. Meystre, Ann. Phys. (Berlin) **525**, 215 (2013).
[5] M. Aspelmeyer, T. J. Kippenberg, and F. Marquardt, Rev. Mod. Phys. **86**, 1391 (2014).
[6] H. Xiong, L.-G. Si, X.-Y. Lv, X.-X. Yang, and Y. Wu, Sci. China Phys. Mech. Astron. **58**, 050302 (2015).
[7] T. Rocheleau, T. Ndukum, C. Macklin, J. B. Hertzberg, A. A. Clerk, and K. C. Schwab, Nature (London) **463**, 72 (2010).
[8] J. Chan, T. P. Mayer Alegre, A. H. Safavi-Naeini, J. T. Hill, A. Krause, S. Gröblacher, M. Aspelmeyer, and O. Painter, Nature (London) **478**, 89 (2011).
[9] J. D. Teufel, T. Donner, D. Li, J. W. Harlow, M. S. Allman, K. Cicak, A. J. Sirois, J. D. Whittaker, K. W. Lehnert, and R. W. Simmonds, Nature (London) **475**, 359 (2011).
[10] E. Verhagen, S. Deléglise, S. Weis, A. Schliesser, and T. J. Kippenberg, Nature (London) **482**, 63 (2012).
[11] V. Fiore, Y. Yang, M. C. Kuzyk, R. Barbour, L. Tian, and H. Wang, Phys. Rev. Lett. **107**, 133601 (2011).
[12] Y.-D. Wang and A. A. Clerk, Phys. Rev. Lett. **108**, 153603 (2012).
[13] C. Dong, V. Fiore, M. C. Kuzyk, and H. Wang, Science **338**, 1609 (2012).
[14] M. Schmidt, M. Ludwig, and F. Marquardt, New. J. Phys. **14**, 125005 (2012).
[15] K. Stannigel, P. Komar, S. J. M. Habraken, S. D. Bennett, M. D. Lukin, P. Zoller, and P. Rabl, Phys. Rev. Lett. **109**, 013603 (2012).
[16] H.-K. Li, X.-X. Ren, Y.-C. Liu, and Y.-F. Xiao, Phys. Rev. A **88**, 053850 (2013).
[17] Y. Yan, W. J. Gu, and G. X. Li, Sci. China Phys. Mech. Astron. **58**, 050306 (2015).
[18] M. D. LaHaye, O. Buu, B. Camarota, and K. C. Schwab, Science **304**, 74 (2004).
[19] J. D. Teufel, R. Donner, M. A. Castellanos-Beltran, J. W. Harlow, and K. W. Lehnert, Nat. Nanotechnol. **4**, 820 (2009).
[20] A. G. Krause, M. Winger, T. D. Blasius, Q. Lin, and O. Painter, Nat. Photon. **6**, 768 (2012).
[21] Y.-W. Hu, Y.-F. Xiao, Y.-C. Liu, and Q. Gong, Front. Phys. **8**, 475 (2013).
[22] L. F. Buchmann, H. Jing, C. Raman, and P. Meystre, Phys. Rev. A **87**, 031601(R) (2013).
[23] T. P. Purdy, R. W. Peterson, and C. A. Regal, Science **339**, 801 (2013).
[24] O. Romero-Isart, A. C. Pflanzer, F. Blaser, R. Kaltenbaek, N. Kiesel, M. Aspelmeyer, and J. I. Cirac, Phys. Rev. Lett. **107**, 020405 (2011).
[25] B. Pepper, R. Ghobadi, E. Jeffrey, C. Simon, and D. Bouwmeester, Phys. Rev. Lett. **109**, 023601 (2012).
[26] M. P. Blencowe, Phys. Rev. Lett. **111**, 021302 (2013).
[27] P. Sekatski, M. Aspelmeyer, and N. Sangouard, Phys. Rev. Lett. **112**, 080502 (2014).
[28] I. Wilson-Rae, N. Nooshi, W. Zwerger, and T. J. Kippenberg, Phys. Rev. Lett. **99**, 093901 (2007).
[29] F. Marquardt, J. P. Chen, A. A. Clerk, and S. M. Girvin, Phys. Rev. Lett. **99**, 093902 (2007).
[30] C. Genes, D. Vitali, P. Tombesi, S. Gigan, and M. Aspelmeyer, Phys. Rev. A **77**, 033804 (2008).
[31] I. Wilson-Rae, N. Nooshi, J. Dobrindt, T. J. Kippenberg, and W. Zwerger, New J. Phys. **10**, 095007 (2008).
[32] Y.-C. Liu, R.-S. Liu, C.-H. Dong, Y. Li, Q. Gong, and Y.-F. Xiao, Phys. Rev. A **91**, 013824 (2015).
[33] F. Elste, S. M. Girvin, and A. A. Clerk, Phys. Rev. Lett. **102**, 207209 (2009).
[34] M. Li, W. H. P. Pernice, and H. X. Tang, Phys. Rev. Lett. **103**, 223901 (2009).
[35] A. Xuereb, R. Schnabel, and K. Hammerer, Phys. Rev. Lett. **107**, 213604 (2011).
[36] T. Weiss and A. Nunnenkamp, Phys. Rev. A **88**, 023850 (2013).
[37] M.-Y. Yan, H.-K. Li, Y.-C. Liu, W.-L. Jin, and Y.-F. Xiao, Phys. Rev. A **88**, 023802 (2013).
[38] T. Ojanen and K. Børkje, Phys. Rev. A **90**, 013824 (2014).
[39] Y.-C. Liu, Y.-F. Xiao, X. S. Luan, and C. W. Wong, Sci. China Phys. Mech. Astron. **58**, 050305 (2015).
[40] Y. Guo, K. Li, W. Nie, and Y. Li, Phys. Rev. A **90**, 053841 (2014).
[41] Y.-C. Liu, Y.-F. Xiao, X. Luan, Q. Gong, and C. W. Wong, Phys. Rev. A **91**, 033818 (2015).
[42] W.-j. Gu and G.-x. Li, Phys. Rev. A **87**, 025804 (2013).
[43] C. Genes, H. Ritsch, and D. Vitali, Phys. Rev. A **80**, 061803(R) (2009).
[44] K. Hammerer, K. Stannigel, C. Genes, P. Zoller, P. Treutlein, S. Camerer, D. Hunger, and T. W. Hänsch, Phys. Rev. A **82**, 021803(R) (2010).
[45] C. Genes, H. Ritsch, M. Drewsen, and A. Dantan, Phys. Rev. A **84**, 051801(R) (2011).
[46] S. Camerer, M. Korppi, A. Jöckel, D. Hunger, T. W. Hänsch, and P. Treutlein, Phys. Rev. Lett. **107**, 223001 (2011).
[47] B. Vogell, K. Stannigel, P. Zoller, K. Hammerer, M. T. Rakher, M. Korppi, A. Jöckel, and P. Treutlein, Phys. Rev. A **87**, 023816 (2013).
[48] F. Bariani, S. Singh, L. F. Buchmann, M. Vengalattore, and P. Meystre, Phys. Rev. A **90**, 033838 (2014).
[49] A. Dantan, B. Nair, G. Pupillo, and C. Genes, Phys. Rev. A **90**, 033820 (2014).
[50] J. S. Bennett, L. S. Madsen, M. Baker, H. Rubinsztein-Dunlop, and W. P. Bowen, New J. Phys. **16**, 083036 (2014).
[51] G. Ranjit, C. Montoya, and A. A. Geraci, Phys. Rev. A **91**, 013416 (2015).
[52] T. P. Purdy, D. W. C. Brooks, T. Botter, N. Brahms, Z.-Y. Ma, and D. M. Stamper-Kurn, Phys. Rev. Lett. **105**, 133602 (2010).
[53] H. Ritsch, P. Domokos, F. Brennecke, and T. Esslinger, Rev. Mod. Phys. **85**, 553 (2013).
[54] A. Jöckel, A. Faber, T. Kampschulte, M. Korppi, M. T. Rakher, and P. Treutlein, Nat. Nanotechnol. **10**, 55 (2015).
[55] H.-K. Li, Y.-C. Liu, X. Yi, C.-L. Zou, X.-X. Ren, and Y.-F. Xiao, Phys. Rev. A **85**, 053832 (2012).